ChemPubSoc Europe

DOI: 10.1002/ejic.201601335

EurJIC European Journal of Inorganic Chemistry

Full Paper

Field-Induced SMMs

Field-Supported Slow Magnetic Relaxation in Hexacoordinate Co^{II} Complexes with Easy Plane Anisotropy

Cyril Rajnák,[a] Ján Titiš,[a] Ján Moncoľ,[b] Franz Renz,[c] and Roman Boča*[a]

Abstract: Two mononuclear cobalt(II) complexes containing four equatorial 4-benzylpyridine and two axial chlorido and/or thiocyanato ligands {$[Co[L]_4X_2]$; X = Cl or NCS} possess easy plane magnetic anisotropy, as determined by magnetic susceptibility and magnetization analyses, and confirmed by ab initio calculations (D = +106 and +95 cm^{-1}). AC susceptibility measurements show a slow magnetic relaxation with two or three relaxation branches. The low-frequency pathway occurs at about 1–10 Hz, and it disappears progressively upon heating. The high-frequency mode exists at frequency ranges above 500 Hz. The characteristics of these field-induced single-molecule magnets strongly depend upon the applied magnetic field, which causes a prolongation of the low-frequency relaxation time and a shortening of the high-frequency one. At 1.0 T and 1.9 K the relaxation time for the low-frequency pathway is as slow as 756 or 164 ms for X = Cl or X = NCS, respectively.

Introduction

Single-molecule magnets that are known up to date cover several classes of transition-metal complexes. There are polynuclear and mononuclear, 3d and 4f, heteronuclear 3d–4f, field-induced and field-suppressed, single-mode and multimode relaxation channel systems. Over the past years, an increased interest has been directed to mononuclear 3d complexes mainly for their easy synthesis, stability, and low price.[1] They involve high-spin Cr^{III}, Mn^{III}, Fe^{III}, Fe^{II}, Fe^{I}, Co^{II}, Ni^{I}, and also Ni^{II} complexes.[2–6] The key factor – the magnetic anisotropy – is much easily tuned by a rational synthesis for mononuclear complexes.

Considerable attention has been paid to the class of mononuclear Co^{II} complexes, mostly tetracoordinate, pentacoordinate, and hexacoordinate. These complexes possess a large magnetic anisotropy expressed by the axial zero-field-splitting (ZFS) parameter D. However, the description in terms of the D and E parameters implies that it is legitimate to apply the spin Hamiltonian (SH) formalism, which holds true only for the non-degenerate ground electronic terms of symmetry A or B (point-group irreducible representation); this is the case of quasi-tetrahedral Co^{II} complexes. For pentacoordinate and hexacoordinate complexes, one should be careful, because here also the degenerate ground electronic terms occur: ^4E for the tetragonal pyramidal geometry (coordination number cn = 4 + 1) and ^4E_g for the elongated tetragonal bipyramid (cn = 4 + 2). Application of the SH formalism to magnetic data fitting and/or ab initio calculations for systems with degenerate ground terms is conceptually incorrect, as the SH approach utilizes the non-degenerate perturbation theory.

Results and Discussion

Herein, we report the synthesis, structure, and magnetic properties of two mononuclear complexes of the type $[Co(bzpy)_4X_2]$ with X = Cl (for **1**) and X = NCS (for **2**); bzpy – 4-benzylpyridine (Figure 1). X-ray structure analysis has been performed by stan-

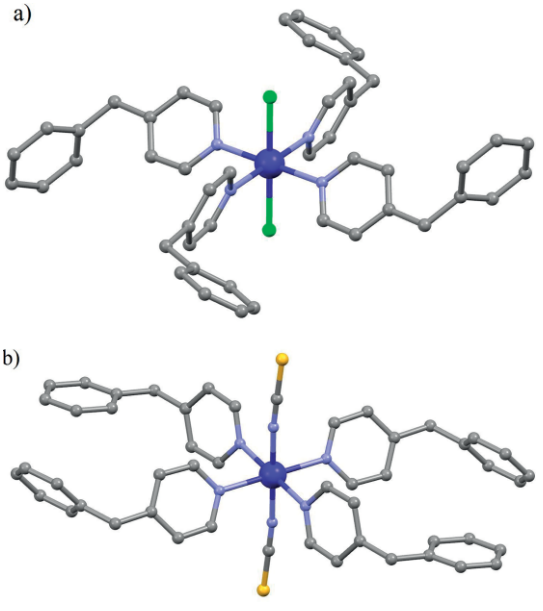

Figure 1. View of the $[Co(bzpy)_4X_2]$ complexes: (a) X = Cl; (b) X = NCS (only one of two crystallographically independent molecules is shown without hydrogen atoms for clarity).

[a] *Department of Chemistry, Faculty of Natural Sciences, University of SS Cyril and Methodius, 91701 Trnava, Slovakia*
E-mail: roman.boca@ucm.sk
http://fpv.ucm.sk/en
[b] *Institute of Inorganic Chemistry, FCHPT, Slovak University of Technology, 81237 Bratislava, Slovakia*
[c] *Institute of Inorganic Chemistry, Leibniz University Hannover, Hannover, Germany*
Supporting information and ORCID(s) from the author(s) for this article are available on the WWW under http://dx.doi.org/10.1002/ejic.201601335.

© 2017 Wiley-VCH Verlag GmbH & Co. KGaA, Weinheim

dard methods, and the crystal data, refinement details, bond lengths, and angles are provided in the Supporting Information.

The complex **1** geometrically resembles an elongated tetragonal bipyramid because of long Co–Cl distances of 2.443 (independent structural unit A) and 2.433 (independent structural unit B) Å relative to equatorial Co–N distances of 2.205 and 2.178 Å, respectively (averaged values are considered). However, the displacements of the metal–ligand distances from their mean values, $d_i = R_i - \bar{R}_i$, are critical and give rise to the structural asymmetry parameter $D_{str} = d_{ax} - d_{eq}$. A negative value of D_{str} means that the electronic behavior of the complex corresponds to that of a compressed tetragonal bipyramid (Table 1) with the $^4A_{2g}$ electronic (mother) term. In such a case, the SH formalism is justified, and the parameter D is proportional to the energy gap Δ between two lowest Kramers doublets Γ_6 (ground) and Γ_7: $\Delta = 2D$.[7] For **2** the coordination polyhedron also refers to the compressed tetragonal bipyramid.

Table 1. Structural and magnetic anisotropy in $[Co(bzpy)_4X_2]$ complexes.[a]

	Independent structural units			
	Unit **1**A	Unit **1**B[b]	Unit **2**A	Unit **2**B
R_{eq} /pm	220.5	217.8	219.8	220.4
R_{ax} /pm	244.3	243.3	208.7	209.4
d_{eq} /pm	2.0	–0.7	1.3	1.9
d_{ax} /pm	–3.2	–4.2	–9.8	–9.1
D_{str} /pm	–5.2	–3.5	–11.1[c]	–11.0[c]
D_{mg} /cm^{-1}	+106		+90.5	
$D_{calcd.}$ /cm^{-1}[c]	+88.6	(+123.8)	+88.6	+90.8
g factors[d]	1.943	(1.478)	1.941	1.946
	2.490	2.049	2.469	2.492
	2.780	2.966	2.788	2.769
g_{iso}	2.405	2.165	2.400	2.403
Δ_I /cm^{-1}[e]	0	0	0	0
	436	91	505	511
	976	780	818	752
$E(\Gamma_i)$ /cm^{-1}[f]	0	0	0	0
	181	259	183	186
	626	446	657	646
	908	785	982	991
	1379	1338	1222	1174
	1457	1353	1350	1314

[a] Mean distances $\bar{R}$(Co–N) = 218.5 and $\bar{R}$(Co–Cl) = 247.5 pm (extracted from the CCDC database). D_{mg}: analysis of susceptibility and magnetization data. [b] Structural unit 1B is non-centrosymmetric, as all its metal–ligand distances are different and the pyridine rings at the *trans*-position are not coplanar. [c] D_{calc}: ab initio calculations (ORCA package). [d] Calculated g factors from effective Hamiltonian. [e] Δ_I: NEVPT2 transition energies (quartet–quartet). [f] $E(\Gamma_i)$: calculated six lowest Kramers doublets (SOC-corrected). Problematic data due to quasi-degeneracy are given in parentheses.

For the structurally characterized complexes **1** and **2**, the magnetic parameters were calculated by using the ab initio CASSCF/NEVPT2/QDPT method (Table 1).[8] The calculated NEVPT2 transition energies Δ_I and their daughter multiplets $E(\Gamma_i)$ corrected for spin–orbit coupling (SOC) confirm that there is not a quasi-degeneracy of the ground term except for the asymmetric unit **1**B (Δ_I = 91 cm^{-1}).

Temperature dependence of the magnetization induced by the static, direct-current (DC) magnetic field has been acquired with a SQUID magnetometer (MPMS-XL7, QuantumDesign) by using the RSO mode of detection. For magnetic susceptibility, the applied field was B_{DC} = 0.1 T, and this was corrected for the underlying diamagnetism and converted into the effective magnetic moment. The effective magnetic moment for **1** adopts a room-temperature value (μ_{eff} = 4.97 μ_B) that is typical for high-spin Co^{II} complexes (Figure 2). On cooling, this value gradually decreases, and at T = 1.9 K it becomes μ_{eff} = 3.60 μ_B. This is a fingerprint of the sizeable zero-field splitting of the $|S, M_S\rangle$ manifolds into two Kramers doublets. The magnetization per formula unit saturates to $M_1 = M_{mol}/N_A\mu_B$ = 2.16 at T = 2.0 K and B = 7.0 T. Such a subnormal value again indicates a substantial zero-field splitting. The magnetic functions for **2** display an analogous course (Supporting Information). Temperature dependence of the molar magnetic susceptibility and field dependence of the molar magnetization at two temperatures were fitted simultaneously to the model of the SH, which yielded D/hc = +106 and +90.5 cm^{-1} for **1** and **2**, respectively. These values match the averaged ZFS parameters predicted by ab initio calculations.

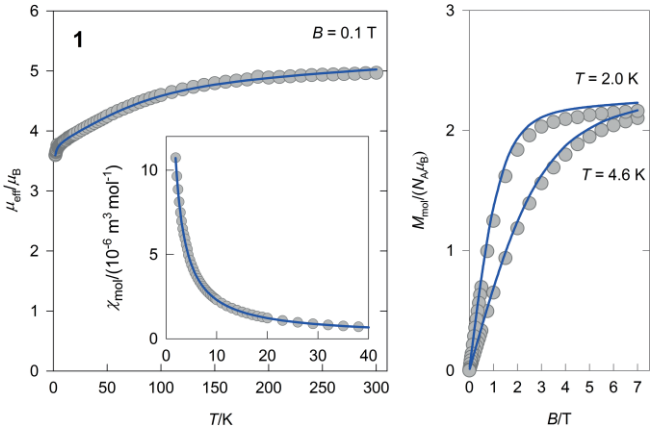

Figure 2. DC magnetic data for **1**. Lines indicate fits with the ZFS model.

The magnetic data induced by the oscillating, alternating-current (AC) magnetic field was taken at an amplitude of B_{AC} = 0.38 mT. The DC field scan for a limited number of frequencies over four decades for **1** shows that at B_{DC} = 0 the out-of-phase component is silent (Figure 3). This confirms a fast magnetic relaxation in the absence of the magnetic field. With increasing DC field up to B_{DC} = 0.5 T, the out-of-phase component varies, but differently for individual frequencies. This confirms that the system shows a field-induced slow magnetic relaxation.

More informative, however, is the frequency dependence of the out-of-phase component for 22 frequencies ranging between 0.1 and 1500 Hz. It can be seen (Supporting Information) that at T = 1.9 K and small-field B_{DC} = 0.2 T there is a dominant relaxation process at about 200 Hz in the high-frequency (HF) region, giving rise to the relaxation time τ(HF) = 0.8 ms. This is accompanied by a satellite peak (visible as a shoulder between 1 to 10 Hz) at the low-frequency (LF) region with τ(LF) = 40 ms.

The former shoulder becomes split when B_{DC} = 0.4 T is applied, indicating that three relaxation channels are open. Now the relaxation time for the LF branch increases to τ(LF) = 394 ms, whereas its counterpart is shortened τ(HF) = 0.3 ms.

© 2017 Wiley-VCH Verlag GmbH & Co. KGaA, Weinheim

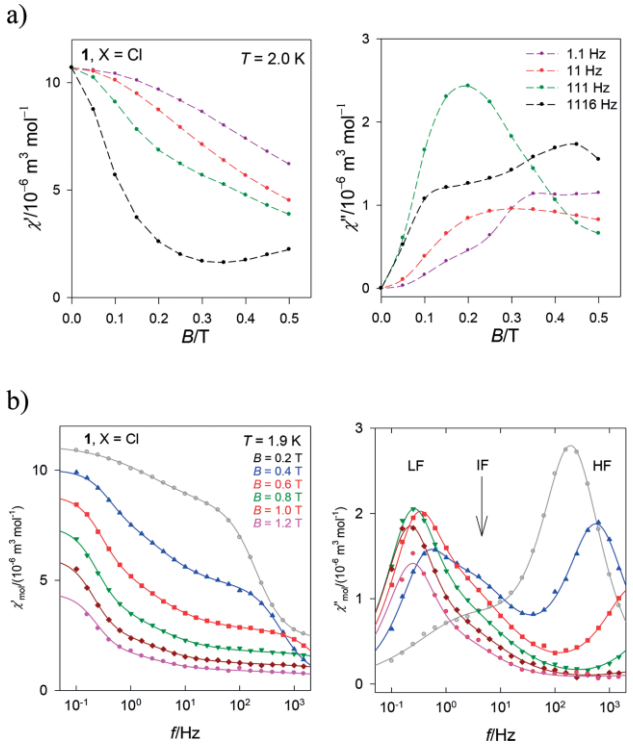

Figure 3. AC susceptibility components for **1**: (a) DC field dependence for a set of fixed frequencies; (b) frequency dependence for fixed fields. The dashed lines are guides for the eyes, the solid lines are fitted.

The intermediate frequency (IF) channel possesses τ(IF) = 43 ms.

This trend (a suppression of the HF branch in favor of the LF branch) continues with increasing external field, as documented by the data listed in Table 2. These were obtained by a simultaneous fit of the in-phase and out-of-phase susceptibility data (44 data points) to the extended three-set Debye model possessing 10 free parameters: three isothermal susceptibilities (χ_{T1}, χ_{T2}, χ_{T3}), three distribution parameters (α_1, α_2, α_3), three relaxation times (τ_1, τ_2, τ_3), and eventually the adiabatic susceptibility χ_S (see the Supporting Information for details). The quality of the fit is assessed by the discrepancy factor for the susceptibility components $R(\chi')$ and $R(\chi'')$ as well as the standard deviation for each free parameter. (When the IF branch is omitted, the AC data cannot be fitted satisfactorily. The IF peak vanishes progressively with the temperature propagation; above 3.5 K it cannot be caught by the data fitting.)

Table 2. Selected AC susceptibility parameters for **1** and **2** at T = 1.9 K and various magnetic fields.

B_{DC} /T	τ_{LF} /10^{-3} s	τ_{IF} /10^{-3} s	τ_{HF} /10^{-6} s	x_{LF}	x_{IF}	x_{HF}
Complex **1**						
0.2		67.1	791	0	0.33	0.67
0.4	394	43.5	273	0.24	0.32	0.44
0.6	541	57.6	52.1	0.34	0.35	0.31
0.8	669	61.4	16.6	0.43	0.34	0.23
1.0	756	50.4	3.0	0.56	0.23	0.20[b]
1.2	681	50.6	3.3	0.60[a]	0.17	0.23
Complex **2**						
0.2	40.2		1300	0.10		0.90
0.4	63.9		282	0.44		0.56
0.6	101		83.4	0.59		0.41
0.8	127		28.5	0.66		0.34
1.0	164		13.2	0.70[a]		0.30[b]

[a] Mole fraction increases with the magnetic field. [b] Mole fraction decreases with the magnetic field.

The isothermal susceptibilities define the mole fraction of the LF, IF, and HF branches: $x_{LF} = (x_{T1} - x_S)/(x_{T3} - x_S)$, $x_{IF} = (x_{T2} - x_{T1})/(x_{T3} - x_S)$, and $x_{HF} = (x_{T3} - x_{T2})/(x_{T3} - x_S)$.

Only x_{LF} increases with the increasing magnetic field, which confirms and quantifies how the low-frequency relaxation mode is supported by the magnetic field. To this end, the relaxation time at B_{DC} = 1.0 T is raised by an order of magnitude to τ(LF) = 756 ms with x_{LF} = 0.56.

A detailed mapping of the frequency dependence of the AC susceptibility components for **1** for a set of constant temperatures is presented in Figure 4 for a representative external magnetic field B_{DC} = 0.6 T. Fitted data (Supporting Information) was used in generating the interpolation and extrapolation lines that are also drawn in Figure 4. These enter the Argand diagram representing three (two) overlapping arcs. The position of the maximum at the out-of-phase susceptibility defines the relaxation time; this is plotted vs. T^{-1} a as an Arrhenius-like graph. Data for the HF branch have been processed by fitting to the extended relaxation equation where, in addition to the Orbach process, also direct, Raman, and quantum tunneling processes take place [Equation (1)]:

$$\tau^{-1} = \tau_0^{-1} \exp(-U/k_B T) + AB^m T + CT^n + D_t \quad (1)$$

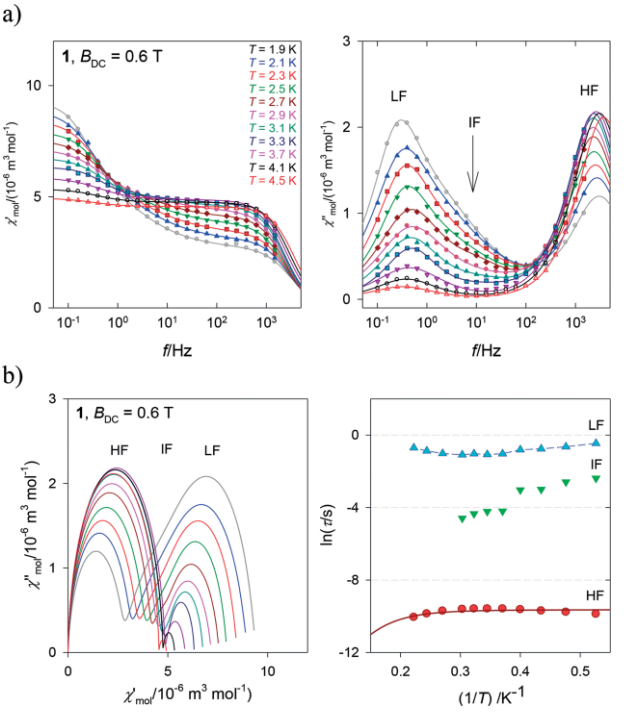

Figure 4. AC susceptibility components for **1**: (a) frequency dependence for fixed temperatures at B_{DC} = 0.6 T; (b) Argand diagram (left) and Arrhenius-like plot (right). The solid lines are fitted. LF: low frequency; IF: intermediate frequency; HF: high frequency.

© 2017 Wiley-VCH Verlag GmbH & Co. KGaA, Weinheim

Table 3. Relaxation parameters for the HF branch in **1** and **2**.[a]

System	Model	B_{DC} /T	D_t /s^{-1}	C /T^{-n} K^{-1} s^{-1} $n = 5$	A /T^{-m} K^{-1} s^{-1} $m = 2$	U/k_B[b]	τ_0 /s
1	Raman	0.4	0.38×10^4	4.16			
1	Raman	0.6	1.33×10^4	5.23			
2	Raman	0.2		3.05	0.96×10^4		
2	Raman	0.4	0.18×10^4	4.29	0.49×10^4		
2	Orbach	0.2			1.19×10^4	22.9	1.16×10^{-6}
2	Orbach	0.4	0.21×10^4		0.50×10^4	27.7	0.31×10^{-6}

[a] The standard deviations are listed in the Supporting Information. [b] U/k_B values are in Kelvin (K).

Parameters A and D_t are effective at low temperature, C in the intermediate range, and τ_0 and U are effective at the high-temperature limit. The obtained parameters are listed in Table 3 by ignoring the Orbach or the Raman process.

There is an unusual feature observed at low temperature for **2**: upon heating from very low temperature (1.9 K), the HF relaxation time no longer stays at the maximum. It starts to increase, passes through a round maximum, and then decreases as normally reported, in accordance with expectations (see the Supporting Information). This effect prevents a successful fitting of the curved Arrhenius-like plot at the low-temperature region by Equation (1), and it thus remains unmodeled so far.

When passing from **1** to **2** it can be seen that the LF and HF peaks of the out-of-phase susceptibility for **2** behave analogously to those for **1** (Figures 5 and 6), though quantitative parameters resulting from the data fitting are different (see the Supporting Information).

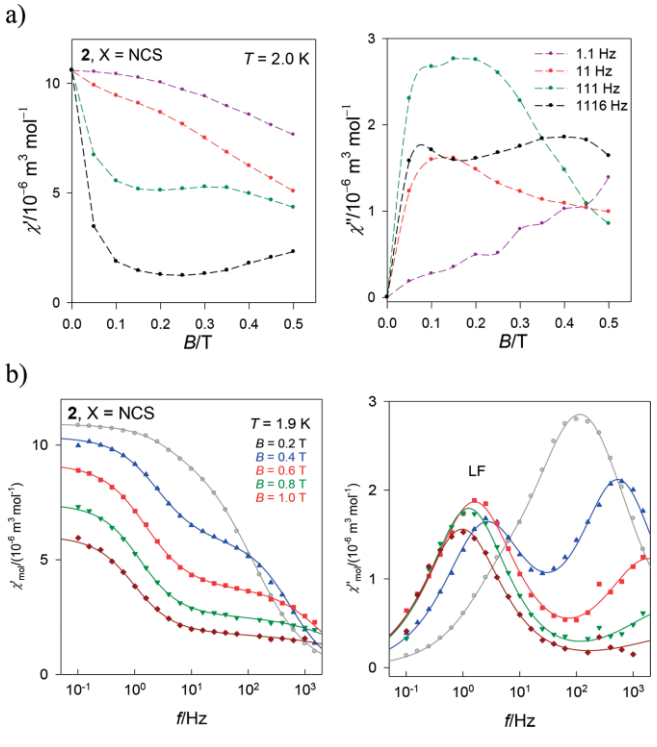

Figure 5. AC susceptibility components for **2** as a function of the magnetic field for a set of fixed frequencies (top) and AC frequency (bottom) for a set of fixed fields. The dashed lines serve as guides for the eyes; the solid lines are fitted.

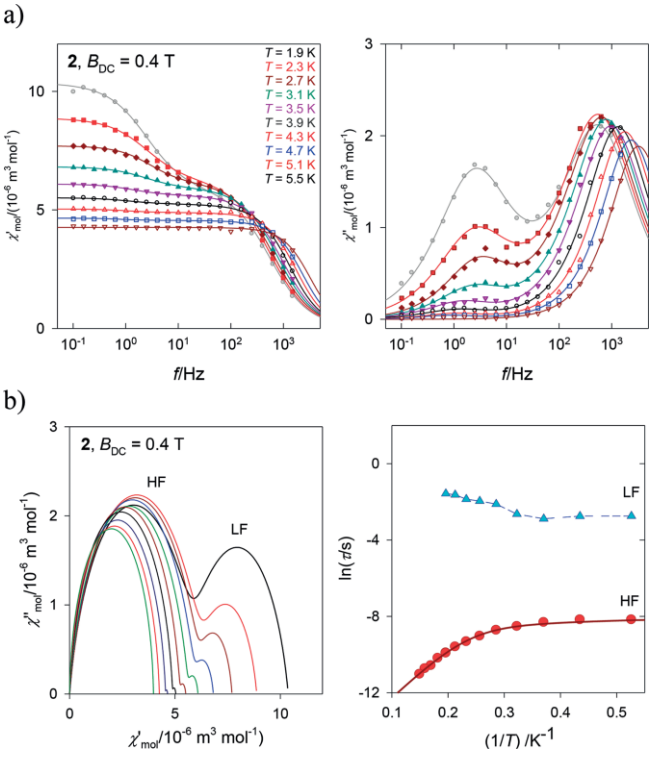

Figure 6. AC susceptibility components for **2**: (a) frequency dependence for fixed temperatures at B_{DC} = 0.4 T. (b) Argand diagram (left) and Arrhenius-like plot (right). The solid lines are fitted. LF: low frequency; HF: high frequency.

The existence of the LF branch is conditioned by some intermolecular interactions that are always present in small complexes containing aromatic rings. They may involve π–π stacking, π–H interactions, or hydrogen bonds. (This is the present case resulting from analysis of hydrogen bonds for **1** and **2** presented in the Supporting Information.) The support of the LF branch of the relaxation by the magnetic field points to its intermolecular nature. The finite "oligomers" in the solid sample can be formed as finite chains, plates, or blocks with averaged coherence length depending upon temperature. The LF branch escapes progressively with temperature as the "oligomers" {Co$_n$} are fragmented into monomers (x_{LF} decreases with temperature). Thus, for high enough temperature only the monomeric units {Co} exhibit the slow relaxation (HF branch). With increasing magnetic field, the concentration of the monomeric units decreases in favor of the oligomers so that they relax more independently of each other. Probably this is the origin of a

© 2017 Wiley-VCH Verlag GmbH & Co. KGaA, Weinheim

higher separation of the LF and HF branches with increasing magnetic field.

On the basis of doping experiments, the intermolecular nature of the LF relaxation channel has also been explored for a heptacoordinate Co^{II} complex with $D > 0$.[5] The extracted value of $U/k_B \approx 50–55$ K for the HF channel is rather unaffected by the degree of doping, which confirms the intramolecular nature of this relaxation. Some groups argue that the hyperfine interaction of the ^{59}Co nuclear spin $I = 7/2$ assists the slow magnetic relaxation in Co^{II} complexes.[9] However, for ^{61}Ni, with a natural abundance of only 1.2 %, $I = 3/2$ holds true, so that the above argument is problematic to accept for Ni^{II}-containing single ion magnets.[6]

Conclusion

The hexacoordinate Co^{II} complexes investigated possess a number of unusual magnetic properties. Both complexes exhibit large magnetic anisotropy expressed by the axial zero-field-splitting parameter $D >> 0$. In such a case of the easy plane anisotropy, the observation of a field-induced slow magnetic relaxation is inconsistent with the Orbach relaxation process; more probable is the relaxation via a Raman process. The field influence on the out-of-phase magnetic susceptibility is very expressive. At low field ($B_{DC} = 0.2$ T) and low temperature ($T = 1.9$ K), a dominant HF relaxation process is registered at frequencies $f > 100$ Hz with an IF satellite. The increase of the field up to 1.0 T causes the suppression of the HF branch in favor of the LF branch: at $T = 1.9$ K and $B = 1.0$ T there is 60 % of the LF mole fraction. At the same time, the LF and HF peaks of the out-of-phase magnetic susceptibility are more separated, which causes a shortening of the HF relaxation time and a sizeable prolongation of the LF relaxation time: τ(LF) = 756 ms for **1** and 164 ms for **2** at $T = 1.9$ K and $B = 1.0$ T. For **1** there is evidence of an intermediate frequency relaxation channel that disappears progressively upon heating.

Experimental Section

Materials and Methods: All chemicals of reagent grade were used as received. Anhydrous $Co(SCN)_2$ and $CoCl_2{\cdot}6H_2O$ were used as sources of Co^{II}. Acetonitrile was used without any further purification. The manipulations were carried out under aerobic conditions. The products were filtered through ashless paper and fritted glass with porosity no. 4.

Physical Measurements: Elemental analyses were carried out with Flash 2000 CHNSO apparatus (Thermo Scientific). Melting points were studied with thermomicroscopy by using a Kofler hot-stage microscope at 4 °C min^{-1}. The solid samples for FTIR measurements were not dried prior to use, and freshly synthesized samples were used. The samples were placed on an ATR holder with highly effective diamond crystal to record spectra in the region 4000–400 cm^{-1} (Nicolet 5700, Thermo Electron) with a DTGS/KBr detector. Far-IR spectra for samples in polyethylene pellets were recorded in the region 50–600 cm^{-1} (Nicolet apparatus). Absorption UV/Vis spectra for liquid samples were recorded by using a UV/Vis/NIR spectrophotometer 50 Bio (Varian) with scan rate 300 nm/min. UV/Vis spectra for solid samples dispersed in Nujol oil were measured by using a Specord 250 Plus (Analytica Jena) instrument with a DAD detector. Conductances were measured with an analogue conductometer OK-112 (Radelkis), and the results were transformed to molar conductivity κ (0.1 M KCl) in units of Sm^{-1}.

$[Co(4\text{-bzpy})_4Cl_2]$ (1): A 100 cm^3 round-bottomed flask was charged with $CoCl_2{\cdot}6H_2O$ (0.053 g, 0.22 mmol) and acetonitrile (20 cm^3). The solution was stirred to form its blue and transparent color at room temperature. After half an hour, 4-benzylpyridine (0.141 cm^3, 0.88 mmol) was added without color change. The reaction mixture was heated with an oil bath for 3 h at 80 °C. Part of the solvent was removed by reduced pressure. Pink crystalline plates were obtained by slow concentration at room temperature in three days. Yield: 0.112 g, 63 %. Melting point: 140–142 °C. $C_{48}H_{44}N_4Cl2Co$ (806.73): calcd. C 71.46, H 5.50, N 6.94; found C 71.03, H 5.48, N 7.01. Λ_m (CH3CN, 25 °C) (κ, 10^{-4} Sm^{-1}): 10.3 (3.83) 10^{-2} S m^2 mol^{-1}. Selected IR bands (ATR): $\tilde{\nu}$ = 3062, 3034, 1613 (s), 1600, 1557 (m), 1494 (s), 1451 (m), 1422 (s), 1223 (m), 1070 (m), 1015 (m), 914, 857, 834 (m), 797 (m), 745 (s), 735, 699 (s), 615 (s), 559 (s), 485 (s), 458 (m) cm^{-1} (s = strong, m = medium). Selected IR bands (1.2 mg in 250 mg KBr): $\tilde{\nu}$ = 3053, 3028, 2971, 2921, 1615 (s), 1599, 1557, 1505, 1494 (s), 1453, 1434 (s), 1354, 1227 (s), 1069 (s), 1026 (s), 918, 866, 833, 795 (s), 748, 738, 699 (s), 618 (s), 564 (s), 489 (s) cm^{-1}. UV/Vis (CH3CN) ν_{max} (ε, M^{-1} cm^{-1}): 15.1 (528), 16.3 (649), 17.5 (547) 10^3 cm^{-1}. UV/Vis (Nujol) ν_{max} (relat. absorb.): 14.993(0.254); 15.723(0.275); 16.42(0.292); 18.116(0.407); 18.975(0.433); 19.763(0.426); 26.042(0.334) 10^3 cm^{-1}.

$[Co(4\text{-bzpy})_4(SCN)_2]$ (2): A 100 cm^3 round-bottomed flask was charged with 4-benzylpyridine (0.141 cm^3, 0.88 mmol), acetonitrile (20 cm^3), and anhydrous $Co(NCS)_2$ (0.039 g, 22 mmol). The reaction mixture changed color gradually to intensive blue. It was heated with an oil bath for 4 h at 80 °C. A part of the solvent was removed by using a rotary evaporator. Pink crystalline needles were obtained by slow concentration at room temperature in two days. Yield: 0.136 g, 72 %. Melting point: 205–207 °C. $C_{50}H_{44}N_6CoS_2$ (851.99): calcd. C 70.49, H 5.21, N 9.86, S 7.53; found C 70.09, H 5.31, N 9.86, S 7.31. Λ_m (CH3CN, 25 °C) (κ, 10^{-4} Sm^{-1}): 27.6 (9.56) 10^{-2} S m^2 mol^{-1}. Selected IR bands (ATR): $\tilde{\nu}$ = 3084, 3026, 2910, 2063 (s) νas(CN from SCN), 1610 (s), 1601, 1558 (m), 1495 (s), 1450 (m), 1419 (s), 1224 (m), 1213, 1204, 1074, 1064 (m), 1014 (s), 860 (m), 838 (m), 798 (s), 751 (m), 733 (s), 704 (s), 697, 617 (s), 560 (s), 486 (s), 459(m) cm^{-1} (s = strong, m = medium). UV/Vis (CH3CN) νmax/10^3 cm^{-1} (ε, M^{-1} cm^{-1}): 16.0 (1132), 17.7 (881), 30.5 (8525) 10^3 cm^{-1}. UV/Vis (Nujol) νmax/10^3 cm^{-1} (relat. absorb.): 9.9(0.260); 16.3(0.248); 18.4(0.352); 20.3(0.418); 26.0(0.561) 10^3 cm^{-1}.

Ab Initio Calculations: Ab initio calculations were performed with the ORCA 3.0.3 computational package at the experimental geometries determined by X-ray diffraction for mononuclear entities. Relativistic effects were included in the calculations by zero-order regular approximation (ZORA) together with the scalar relativistic contracted version of TZVP basis functions. The calculations of ZFS parameters were based on state-averaged complete active-space self-consistent field (SA-CASSCF) wave functions complemented by N-electron valence second-order perturbation theory (NEVPT2). The active space of the CASSCF calculations comprises seven electrons in five metal-based d orbitals. The state-averaged approach was used, in which all ten quartet states and forty doublet states were equally weighted. The calculations utilized the RI approximation with appropriate decontracted auxiliary basis sets and the chain-of-spheres (RIJCOSX) approximation to exact exchange. Increased integration grids (Grid4) and tight SCF convergence criteria were used. The ZFS parameters were calculated through quasi-degenerate perturbation theory in which an approximation to the Breit–

© 2017 Wiley-VCH Verlag GmbH & Co. KGaA, Weinheim

Pauli form of the spin–orbit coupling operator (SOMF) and the effective Hamiltonian theory were utilized.

Structural Data

The intensity data was collected with a Rigaku XtaLAB diffractometer with AFC11 partial χ geometry goniometer, equipped with a Saturn 724+ HG CCD detector at 120 K. Mo-K_α radiation (λ = 0.71075 Å, MicroMax-007HF DW rotating anode source, multilayer optic VariMax DW) was used for the measurement. The diffraction intensities were corrected for Lorentz, polarization, and absorption effects; data collection, cell parameters, and data reduction were initially carried out by using the Crystal Clear software. The structures were solved by direct methods with SHELXT,[10] or by the charge-flipping method SuperFlip,[11] refined by a full-matrix least-squares procedure with SHELXL (ver. 2016/4),[12] or Olex2.refine,[13] and drawn with the OLEX2 package.[14] The U_{iso} of H-atoms have been fixed at 1.2 times of all aromatic C(H) or C(H,H) groups, and all aromatic CH or secondary CH_2 groups have been refined with riding coordinates using AFIX 43 or AFIX 23 commands of the SHELXL or Olex2.refine programs, respectively. All details regarding H-atoms are added in the CIF files in loops "_olex2_refinement_description" and "_iucr_refine_instructions_details".

CCDC 1497488 (for **1**), and 1497489 (for **2**) contain the supplementary crystallographic data for this paper. These data can be obtained free of charge from The Cambridge Crystallographic Data Centre.

Acknowledgments

The Slovak Grant Agency VEGA (VEGA 1/0522/14, VEGA 1/0534/16), The Slovak Research and Development Agency APVV (APVV-14-0078), and the Deutscher Akademischer Austausch Dienst (DAAD) program Germany/Slovakia are acknowledged for financial support. Dr. J. Kožíšek (Slovak University of Technology, Bratislava) and Prof. J. Marek (Brno) are acknowledged for the single-crystal X-ray experiments.

Keywords: Cobalt · Structure elucidation · Magnetic properties · Slow magnetic relaxation · Single-molecule magnets

[1] a) G. A. Craig, M. Murrie, *Chem. Soc. Rev.* **2015**, *44*, **2135**, and references cited therein; b) S. Gómez-Coca, D. Aravena, R. Morales, E. Ruiz, *Coord. Chem. Rev.* **2015**, *289–290*, 379, and references cited therein; c) J. M. Frost, K. L. M. Harriman, M. Murugesu, *Chem. Sci.* **2016**, *7*, 2470, and references therein.

[2] a) W. Huang, T. Liu, D. Wu, J. Cheng, Z. W. Ouyang, C. Duan, *Dalton Trans.* **2013**, *42*, 15326; b) F. Yang, Q. Zhou, Y. Zhang, G. Zeng, G. Li, Z. Shi, B. Wang, S. Feng, *Chem. Commun.* **2013**, *49*, 5289; c) R. Boča, J. Miklovič, J. Titiš, *Inorg. Chem.* **2014**, *53*, 2367; d) M. R. Saber, K. R. Dunbar, *Chem. Commun.* **2014**, *50*, 12266; e) J. M. Zadrozny, J. Liu, N. A. Piro, C. J. Chang, S. Hill, J. R. Long, *Chem. Commun.* **2012**, *48*, 3927; f) J. M. Zadrozny, J. R. Long, *J. Am. Chem. Soc.* **2011**, *133*, 20732; g) J. M. Zadrozny, J. Telser, J. R. Long, *Polyhedron* **2013**, *64*, 209; h) L. Smolko, J. Černák, J. Dušek, J. Miklovič, J. Titiš, R. Boča, *Dalton Trans.* **2015**, *44*, 17565; i) C. Rajnák, A. Packová, J. Titiš, J. Miklovič, J. Moncoľ, R. Boča, *Polyhedron* **2016**, *110*, 85–92.

[3] a) F. Habib, O. R. Luca, V. Vieru, M. Shiddiq, I. Korobkov, S. I. Gorelsky, M. K. Takase, L. F. Chibotaru, S. Hill, R. H. Crabtree, M. Murugesu, *Angew. Chem. Int. Ed.* **2013**, *52*, 11290; *Angew. Chem.* **2013**, *125*, 11500; b) T. Jurca, A. Farghal, P.-H. Lin, I. Korobkov, M. Murugesu, D. S. Richeson, *J. Am. Chem. Soc.* **2011**, *133*, 15814; c) C. Rajnák, J. Titiš, O. Fuhr, M. Ruben, R. Boča, *Inorg. Chem.* **2014**, *53*, 8200; d) A. Packová, J. Miklovič, R. Boča, *Polyhedron* **2015**, *102*, 88; e) I. Nemec, R. Marx, R. Herchel, P. Neugebauer, J. van Slageren, Z. Trávníček, *Dalton Trans.* **2015**, *44*, 15014; f) I. Nemec, H. Liu, R. Herchel, X. Zhang, Z. Trávníček, *Zesz. Nauk. Inst. Ciezkiej Synt. Org.* **2016**, *215*, 158; g) I. Nemec, R. Herchel, Z. Trávníček, *Dalton Trans.* **2016**, *45*, 12479.

[4] a) J. Vallejo, I. Castro, J. Ruiz-García, J. Cano, M. Julve, F. Lloret, G. De Munno, W. Wernsdorfer, E. Pardo, *J. Am. Chem. Soc.* **2012**, *134*, 15704; b) E. Colacio, K. Ruiz, E. Ruiz, E. Cremades, J. Krzystek, S. Carretta, J. Cano, T. Guidi, W. Wernsdorfer, E. K. Brechin, *Angew. Chem. Int. Ed.* **2013**, *52*, 9130; *Angew. Chem.* **2013**, *125*, 9300; c) Y.-Y. Zhu, C. Cui, Y.-Q. Zhang, J.-H. Jia, X. Guo, C. Gao, K. Qian, S.-D. Jiang, B.-W. Wang, Z.-M. Wang, S. Gao, *Chem. Sci.* **2013**, *4*, 1802; d) I. A. Gass, S. Tewary, A. Nafady, N. F. Chilton, C. J. Gartshore, M. Asadi, D. W. Lupton, B. Moubaraki, A. M. Bond, J. F. Boas, S.-X. Guo, G. Rajaraman, K. S. Murray, *Inorg. Chem.* **2013**, *52*, 7557; e) M. S. Fataftah, J. M. Zadrozny, D. M. Rogers, D. E. Freedman, *Inorg. Chem.* **2014**, *53*, 10716; f) R. Herchel, L. Váhovská, I. Potočňák, Z. Trávníček, *Inorg. Chem.* **2014**, *53*, 5896.

[5] F. Habib, I. Korobkov, M. Murugesu, *Dalton Trans.* **2015**, *44*, 6368.

[6] J. Miklovič, D. Valigura, R. Boča, J. Titiš, *Dalton Trans.* **2015**, *44*, 12484.

[7] R. Boča, *Struct. Bonding (Berlin)* **2006**, *117*, 1–240.

[8] a) The ORCA program system, F. Neese, *Wiley Interdiscip. Rev.: Comput. Mol. Sci.* **2012**, *2*, 73; b) F. Neese, *ORCA* – An Ab Initio, Density Functional and Semi-empirical Program Package, version 3.0.3, **2014**; c) M. Atanasov, D. Ganyushin, D. A. Pantazis, K. Sivalingam, F. Neese, *Inorg. Chem.* **2011**, *50*, 7460; d) C. Angeli, S. Borini, M. Cestari, R. Cimiraglia, *J. Chem. Phys.* **2004**, *121*, 4043; e) C. Angeli, R. Cimiraglia, S. Evangelisti, T. Leininger, J.-P. Malrieu, *J. Chem. Phys.* **2001**, *114*, 10252; f) C. Angeli, R. Cimiraglia, J.-P. Malrieu, *J. Chem. Phys.* **2002**, *117*, 9138; g) F. Neese, *J. Chem. Phys.* **2005**, *122*, 34107; h) D. Ganyushin, F. Neese, *J. Chem. Phys.* **2006**, *125*, 24103; i) F. Neese, *J. Chem. Phys.* **2007**, *127*, 164112.

[9] S. Gómez-Coca, A. Urtizberea, E. Cremades, J. P. Alonso, A. Camón, E. Ruiz, L. Ruiz, *Nature Commun.* **2014**, *5*, 4300.

[10] G. M. Sheldrick, *Acta Crystallogr., Sect. A* **2015**, *71*, 3.

[11] L. Palatinus, G. Chapuis, *J. Appl. Crystallogr.* **2007**, *40*, 786.

[12] G. M. Sheldrick, *Acta Crystallogr., Sect. C* **2015**, *71*, 3.

[13] L. J. Bourhis, O. V. Dolomanov, L. J. Gildea, J. A. K. Howard, H. Puschmann, *Acta Crystallogr., Sect. A* **2015**, *71*, 59.

[14] O. V. Dolomanov, L. J. Bourhis, L. J. Gildea, J. A. K. Howard, H. Puschmann, *J. Appl. Crystallogr.* **2009**, *42*, 339.

Received: November 7, 2016

© 2017 Wiley-VCH Verlag GmbH & Co. KGaA, Weinheim